Int. J. Electrochem. Sci., 7 **(2012)** 10282 - 10290

International Journal of
ELECTROCHEMICAL
SCIENCE
www.electrochemsci.org

Effects of Quenching Rate on Microstructure and Electrochemical Properties of $(Mg_{70.6}Ni_{29.4})_{92}La_8$ Alloys

Huang Lin-jun[*], *Wang Yan-xin*, *Tang Jian-guo*[*], *Liu Jing-quan*, *Wang Yao*, *Liu Ji-xian*

College of Chemistry, Chemical and Environmental Engineering, Qingdao University, Qingdao 266071, China)
[*]E-mail: newboy66@126.com (Huang Lin-jun); tang@qdu.edu.cn (Tang Jian-guo)

Received: 15 August 2012 / *Accepted:* 6 September 2012 / *Published:* 1 October 2012

Amorphous and nanocrystalline $(Mg_{70.6}Ni_{29.4})_{92}La_8$ alloys were prepared by rapid solidification. The microstructure of the as-quenched ribbons and the electrochemical properties of these alloys with different velocity of cooling roll were characterized and measured. The experimental results showed that the degree of short-range order and the discharge-capacity increased with increasing velocity of cooling roll for $(Mg_{70.6}Ni_{29.4})_{92}La_8$ alloys. The highest discharge capacity reached 568.5 mAh g^{-1} for $(Mg_{70.6}Ni_{29.4})_{92}La_8$ sample with the velocity of 21.8m·s^{-1}. It's capacity conservation rate was 79.3% after 10 cycles. It is obvious that Mg_2NiH_4 phase forms during the charging process. The amorphous background concealed by the strong Nipeaks shows much amorphous phase remains. It indicated that the amorphous structure was a key factor to achieve high discharge capacity and good cycling stability.

Keywords: Mg-Ni-La hydrogen-storage alloy; microstructure; Electrochemical properties; Melt-Spinning.

1. INTRODUCTION

Mg_2Ni-type intermetallic compounds are the most promising materials for hydrogen storage [1] and Ni-MH batteries [2] owing to their abundance, light weight, and high hydrogen capacity, e.g. 3.6 wt.% for Mg_2NiH_4, 4.5 wt.% for Mg_2CoH_5 and 5.4 wt.% for Mg_2FeH_6. However, these kinds of the hydrides suffer from high thermodynamic stability, resulting in sluggish hydriding/dehydriding kinetics which makes them still far from practical applications. The hydrogen storage kinetics of the Mg-based alloy is strongly dependent upon the nature of its alloying elements and structure. It is reported that the use of various non-equilibrium processing techniques such as mechanical alloying (MA) [3,4] and melt quenching [5] has improved the hydrogen absorption and desorption kinetics ofMgand Mg-based alloys by virtue of the formation of a nanocrys-talline or nano-amorphous

structure. As reported by Wu et al. [6], the kinetics of the hydrogen absorption/desorption reactions of the melt-spun Mg–10Ni–2Mm (at.%) alloy ribbons was greatly improved by increasing the quenching rate, and amaximum hydrogen storage capacity of 5.1 wt.% H was obtained. Lang et al. [7] reported that severe plastic deformation performed by a vertical cold rolling apparatus could be used to enhance hydrogen sorption properties of metal hydrides. The hydrogen sorption kinetics of magnesium hydride, after only five rolling passes, was greatly enhanced without noticeable loss of capacity. Kalinichenka et al. [8] testified that Mg–Cu–Ni–Y system alloys, prepared by melt spinning technology, can reach reversible gravimetric hydrogen storage densities of up to 4.8 wt.% H2.

Although remarkable progress has been achieved for overcoming the above-mentioned drawbacks, the practical applications of the Mg2Ni-type hydrides as the negative electrode of the Ni-MH battery are largely frustrated by their extremely poor electrochemical cycle stability. The key challenge faced by the researches in this area still remains intact, enhancing electrochemical cycle stability and reducing the thermodynamic stability of the hydrides.

In a series of our previous papers the crystallization, microstructure and the hydrogen storage properties for various rapidly Mg-based amorphous alloys were studied [9–12]. This paper is a further study aiming to give a detailed investigation on the effects of quenching rate on microstructure of $(Mg_{70.6}Ni_{29.4})_{92}La_8$ Alloys and the effects of microstructure on the discharge capacity are also discussed.

2. EXPERIMENTAL

$(Mg_{70.6}Ni_{29.4})_{92}La_8$ alloy ingot was prepared by induction melting a mixture of pure La metal and Mg-Ni alloy in a vacuum furnace under the protection of argon gas. Based on the low melting point and the high vapor pressure of Mg, a special melting technique, that is positive pressure protection and repeated melting, has to be taken to prevent massive Mg evaporation and ensure composition homogeneity during master alloy ingot preparation. The amorphous ribbons were produced by a single roller melt-spun technique(copper quenching disc with a diameter of 250mm and surface velocity of about 5~25ms^{-1}) in a argon atmosphere of 400mbar. The ribbons were about 2mm wide and 20 μm thick.

In electrochemical measurement, the amorphous alloy ribbons were fixed in a special mold to form the negative electrode. The positive electrode was made of Ni-oxyhydroxide/dihydroxide. The alkaline solution was 6mol/l KOH containing 20g/l LiOH. The specimens were charged at 100mA/g for 12h and discharged at 50mA/g using the BTW-2000 battery testing instrument (Arbin). The discharged cut-off potential was set to 0.8 V between the two electrodes. The resting time between the charge and discharge was 1 h.

The microstructural characterization of the ribbons after charge/discharge cycles was confirmed by high resolution transmission electron microscopy (HRTEM, JEOL-2010) and by X-ray(using Cu k_α radiation) and electron diffraction.

3. RESULTS AND DISCUSSION

3.1 Effects of quenching rate on microstructure

The XRD patterns of the $(Mg_{70.6}Ni_{29.4})_{92}La_8$ samples with different quenching rate are presented in Fig.1. It is seen that the as-quenched$(Mg_{70.6}Ni_{29.4})_{92}La_8$ alloys experienced a structural transformation from the nanocrystalline to the amorphous with the increasing of quenching rate. $(Mg_{70.6}Ni_{29.4})_{92}La_8$ alloy shows a nanocrystalline structure with some amorphous phases when the quenching rate is 5.2ms^{-1}. By indexing, the nano-crystalline phase Mg_2Ni and $LaMg_2Ni_9$ are detected. When the quenching rate exceeds 6.4ms^{-1}, the alloys $(Mg_{70.6}Ni_{29.4})_{92}La_8$ all show only a broad and diffuse peak, namely the featureless appearance is typical of amorphous structure. It is also seen from Fig.1 that the typical amorphous peaks get low and even with the quenching rate increasing, which implies more uniform of elements in the amorphous structure.

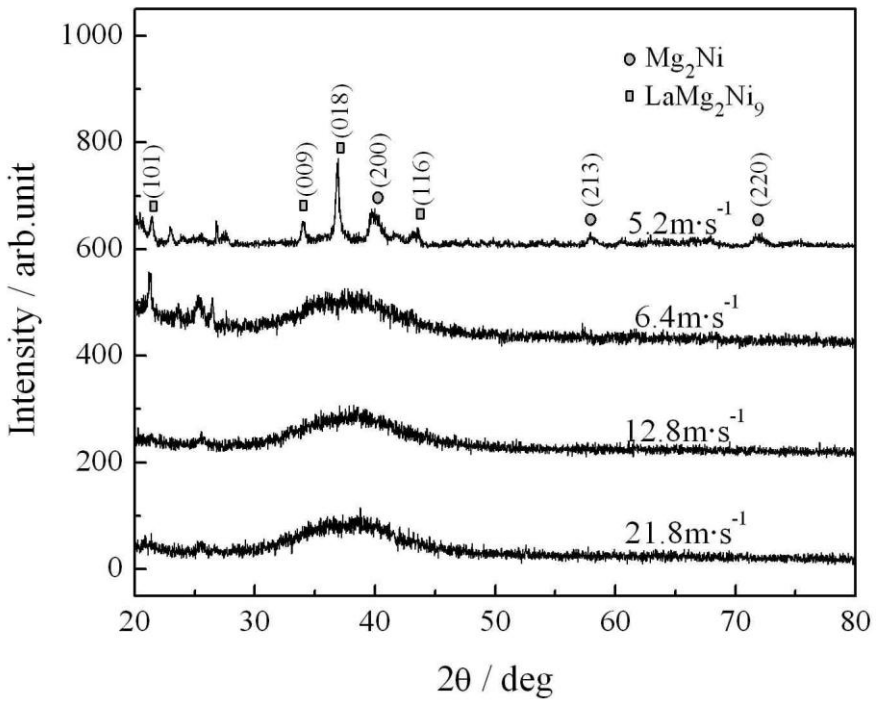

Figure 1. X-ray diffraction patterns of Mg-Ni-La alloys with different quenching rate

According to Scherrer formula, Table 1 gives the results of short-range order for amorphous alloys with different quenching rate. It can be seen from Table 1, with the quenching rate increases, the short-range orde for different ribbons becomes small. That means the increasing of quenching rate strengthen the degree of alloy amorphization .

Fig. 2 shows the high-resolution transmission electron microscopy images of samples $(Mg_{70.6}Ni_{29.4})_{92}La_8$ with different quenching rate.

Table 1. The short-range order of amorphous alloys with different quenching rate

quenching rate / $m \cdot s^{-1}$	short-range order / nm
6.4	1.100
12.8	1.077
21.8	1.059

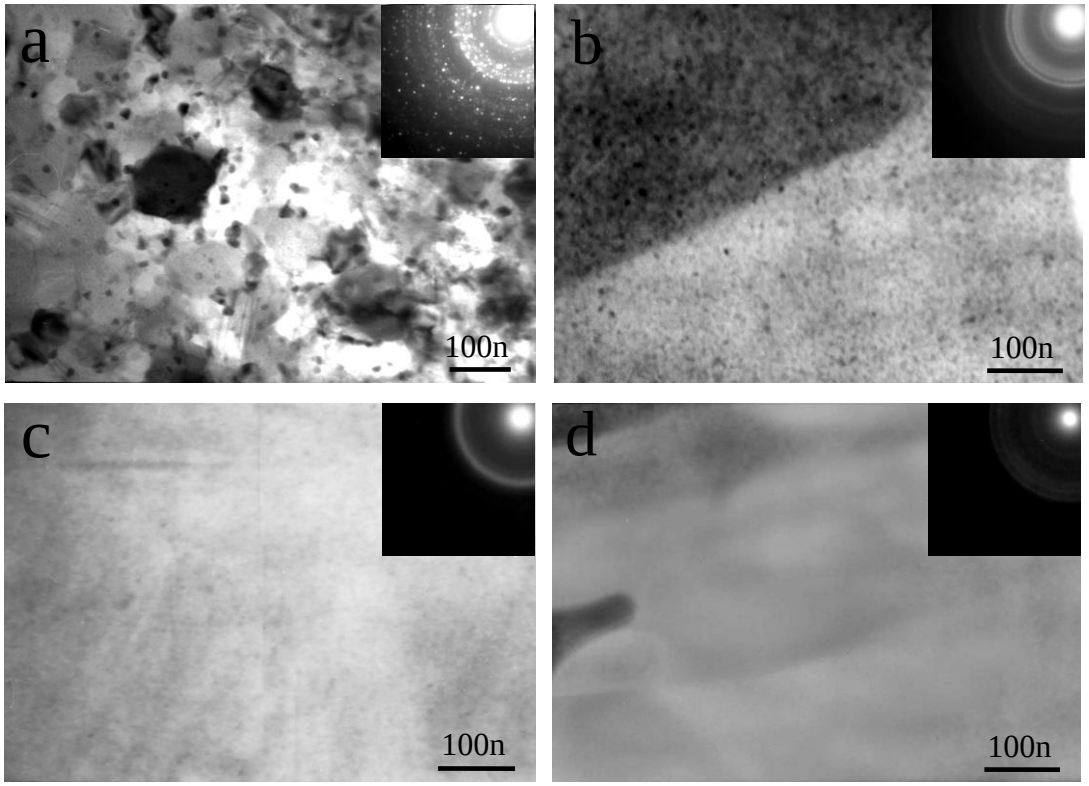

Figure 2. TEM image and electron diffraction pattern of Mg-Ni-La alloys with (a) 5.2 $m \cdot s^{-1}$ (b) 6.4 $m \cdot s^{-1}$ (c) 12.8 $m \cdot s^{-1}$ (d) 21.8 $m \cdot s^{-1}$ quenching rate

It showed that an nano-crystalline structures with a few residual amorphous phases was abtained in Fig. 2 a. with a 5.2 $m \cdot s^{-1}$ quenching rate and crystalline phase Mg_2Ni and $LaMg_2Ni_9$ with average grain size in the range 50–80nm. The TEM image of as-quenched alloy with 6.4 $m \cdot s^{-1}$ quenching rate is shown in Fig.2 b. It was found that the nano-crystalline structures with average grain size in the range 10–20nm was detected and a typical wide diffraction ring of amorphous structure presented in the XRD pattern. It was presumed that the nanocrystalline was embedded in the amorphous matrix. The Fig.2 c and d shows the TEM image and electron diffraction pattern of as-quenched $(Mg_{70.6}Ni_{29.4})_{92}La_8$ alloy with 12.8 $m \cdot s^{-1}$ and 21.8 $m \cdot s^{-1}$quenching rate , it were found that a uniform amorphous structure were obtained.

3.2 Effects of quenching rate on electrochemical property

Fig. 3 shows the variation of the discharge capacity of the different samples versus the number of cycles. It can be observed that whatever the cycle number is, $(Mg_{70.6}Ni_{29.4})_{92}La_8$ with a 21.8 $m \cdot s^{-1}$ quenching rate has the highest capacity and 5.2$m \cdot s^{-1}$ quenching rate has the lowest one. For each quenching rate, with increasing cycle numbers the discharge capacity to reach a maximum after three or four cycles, and then decreases for upper cycle numbers. The curves of the discharge capacity turn to smooth after 6 cycles. The largest discharge capacity of samples reached 177.5 $mAh \cdot g^{-1}$ for 5.2$m \cdot s^{-1}$ quenching rate, 298.8 $mAh \cdot g^{-1}$ for 6.4$m \cdot s^{-1}$ quenching rate, 531.8 $mAh \cdot g^{-1}$ for 12.8$m \cdot s^{-1}$ quenching rate and 568.5 $mAh \cdot g^{-1}$ for 21.8$m \cdot s^{-1}$ quenching rate.

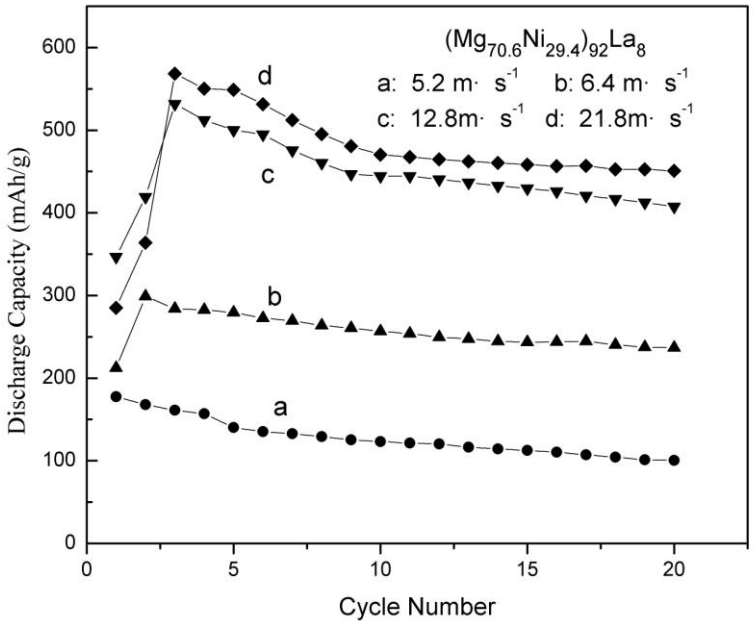

Figure 3. Variation of the discharge capacity vs. the cycle number for the $(Mg_{70.6}Ni_{29.4})_{92}La_8$ samples with different quenching rate.

Fig. 4 gives the variation, as function of the quenching rate, of the maximum discharge capacity (Cmax) and the discharge capacity after 20 cycles (C20). After 20 cycles, the discharge capacity C20 reaches 56.7%（5.2$m \cdot s^{-1}$）, 79.2%（6.4$m \cdot s^{-1}$）,76.7 %（12.8$m \cdot s^{-1}$） and 79.3%（21.8 $m \cdot s^{-1}$） of the discharge capacity Cmax .From above results, it is considered that the increase of discharge capacities is not only a function of the sample composition but strongly influenced by the amorphous phase proportion in the alloyed material. As the content of Nd increases, the diffraction peak at about 40◦ shifts to lower angle (Fig. 1), this suggests the disordered degree of their structures increased [13]. That would enhance hydrogen diffusivity and solubility in amorphous and disordered structures, associated with the wide energy distribution of the available sites for hydrogen in the glassy structure as well as avoiding the long-range diffusion of hydrogen through an already formed hydride.

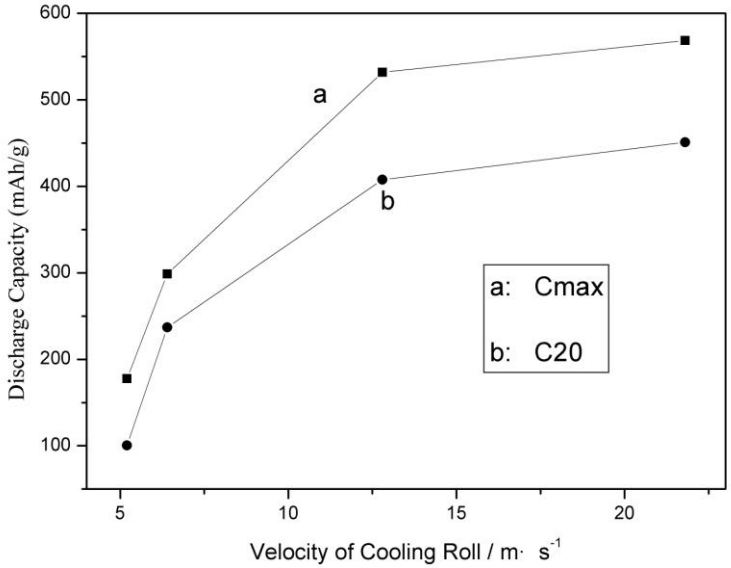

Figure 4. The relationship between the discharge capacity and the quenching rate for the $(Mg_{70.6}Ni_{29.4})_{92}La_8$ samples.

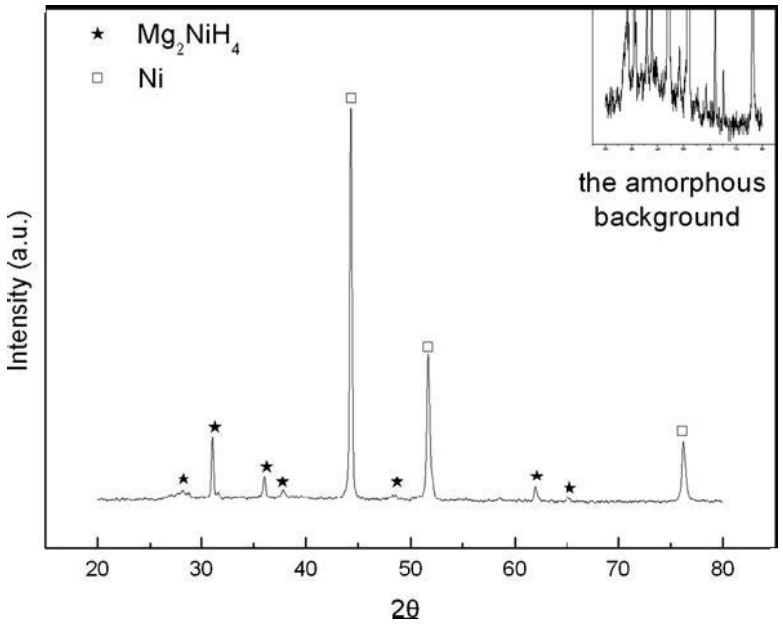

Figure 5. XRD patterns of amorphous $(Mg_{70.6}Ni_{29.4})_{92}La_8$ alloy charged at 3 cycle. clesdischarge capacity vs. the cycle number for the different samples.

.

Fig. 5 shows the XRD patterns of the charged $(Mg_{70.6}Ni_{29.4})_{92}La_8$ sample with a 21.8 $m \cdot s^{-1}$ quenching rate for three cycles. Because the sample contains 50 wt.% of nickel powder, three strong characteristic diffraction peaks of Ni are present. It is obvious that Mg_2NiH_4 phase forms during the charging process. The amorphous background concealed by the strong Ni peaks shows some amorphous phase remains. The crystallinity of $(Mg_{70.6}Ni_{29.4})_{92}La_8$ alloy calculated from Fig. 5 is about 74%, that is, the percentage of residual amorphous phase is 26%. The H atoms in the alloy are mainly

stored in two regions, i.e. one part in the amorphous phase and the other part in the Mg_2NiH_4 phase. The crystallization behavior of the $(Mg_{70.6}Ni_{29.4})_{92}La_8$ alloy after hydrogenation is different from the result reported by Spassov and Koster [14], which showed that the hydrogenation slightly decreased the thermal stability but strongly influenced the secondary crystallization of the as-quenched amorphous $Mg_{87}Ni_{12}Y_1$ alloy.

The relationship of discharge potentials (voltage) and the discharge capacities (at the 10th cycle) is shown in Fig. 6. It is seen that there is a discharge potential flat from 1.3 to 1.0V for each alloy with variation of the discharge capacity which denotes a range of discharge capacity that the alloy can be used. It is found that the discharge capacities of the discharge potential flats have reached more than 400 $mAhg^{-1}$ for $(Mg_{70.6}Ni_{29.4})_{92}La_8$ sample with a 21.8 and 12.8$m\cdot s^{-1}$ quenching rate. However, the discharge capacity of the discharge potential flat of sample with a 5.2$m\cdot s^{-1}$ quenching rate is only 50 $mAhg^{-1}$. It is also important to point out that the discharge capacity is significantly dependent on the microstructure of the electrode materials.

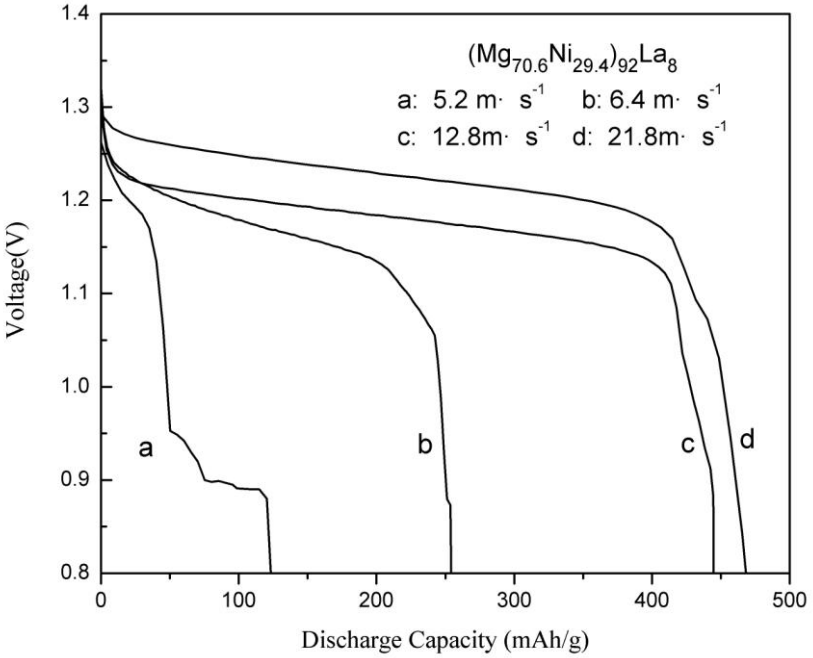

Figure 6. Relationship of voltage and the discharge capacities (at the 10th cycle) for Mg-Ni-La alloys

Xuezhang et al. [15] and Khorkounov et al. [16] reported that the amorphous 2Mg–Fe + 150 wt.%Ni and $Mg_{61}Ni_{30}Y_9$ ribbons were synthesized by mechanical alloying. Wang et al. [17], Xu et al. [18] and Jurczyk et al. [19] also reported respectively that the amorphous $Mg_{1.8}Nd_{0.2}Ni$ (the discharge capacity is 323.5 $mAhg^{-1}$), $PrMgNi_4$ (the discharge capacity is 254 $mAhg^{-1}$) and $Mg_{1.5}Mn0.5Ni$ ribbons (the discharge capacity is 241 $mAhg^{-1}$) were synthesized by mechanical alloying. From the above results, it is evident that the melt–spun ribbon $(Mg_{70.6}Ni_{29.4})_{92}La_8$ (the maximum discharge capacity is 568.5 $mAhg^{-1}$with a 21.8$m\cdot s^{-1}$ quenching rate) showed superior hydrogenation kinetics and higher discharge capacity. One explanation for this could be the homogeneous microstructure of the melt–

spun alloy. The as-cast eutectic alloy charged/discharged for some cycles consisted of lamellae of primary and secondary phases, where long continuous boundaries between primary and secondary phases could act as diffusion paths prior to hydrogen diffusion into the bulk. Zhu et al. [20] also reported that an auto-catalytic effect might govern the hydriding mechanism of the nanophase composite, while the hydriding process of single component alloys proceeds by means of a nucleation and growth mechanism.

4. CONCLUSIONS

Effects of quenching rate on microstructure and electrochemical properties of $(Mg_{70.6}Ni_{29.4})_{92}La_8$ alloys were examined. The results obtained are summarized as follows:

1). The single amorphous phase was obtained in the melt-spun $(Mg_{70.6}Ni_{29.4})_{92}La_8$ ribbons when the quenching rate exceeds $6.4ms^{-1}$.

2). In the cyclic life measurements, the discharge capacities increased with increasing quenching rate. The highest discharge capacity reached more than 568.5 $mAh\cdot g^{-1}$ for $21.8m\cdot s^{-1}$ quenching rate at the discharge current densities of $50mAg^{-1}$ for$(Mg_{70.6}Ni_{29.4})_{92}La_8$ samples and the discharge capacity reaches 79.3% of the maximum discharge capacity after 20 cycles.

3). There is a discharge potential flat from 1.2 to 1.0V for each alloy with variation of the discharge capacity. The discharge capacities of the discharge potential flat have reached more than 400 $mAhg^{-1}$ for $(Mg_{70.6}Ni_{29.4})_{92}La_8$ sample with a 21.8 and $12.8m\cdot s^{-1}$ quenching rate.

4). It indicated that the amorphous structure was a key factor to achieve high discharge capacity and good cycling stability.

ACKNOWLEDGEMENTS

This work was supported by the Ph.D. Fund of Shandong Province(Grant No. BS2009Cl039), Colleges and universities in Shandong Province science and technology projects Fund(Grant No. J11LD03), the technology development projects of Qingdao city(Grant No.12-1-4-2-(17)-jch) and National Nature Science Foundation of China (Grant No. 51273096).

References

1. I.P. Jain, C. Lal, A. Jain, *Int. J. Hydrogen Energy* 35 (2010) 5133–5144.
2. X.Y. Zhao, L.Q. Ma, *Int. J. Hydrogen Energy* 34 (2009) 4788–4796.
3. S.N. Kwon, S.H. Baek, D.R. Mumm, S.H. Hong, M.Y. Song, *Int. J. Hydrogen Energy* 33 (2008) 4586–4592.
4. T. Spassov, P. Delchev, P. Madjarov, M. Spassova, Ts. Himitliiska, *J. Alloys Compd*. 495 (2010) 149–153.
5. P. Palade, S. Sartori, A. Maddalena, G. Principi, S. Lo Russo, M. Lazarescu, G. Schinteie, V. Kuncser, G. Filoti, *J. Alloys Compd*. 415 (2006) 170–176.
6. Y.Wu,M.V. Lototsky, J.K. Solberg, V.A. Yartys,W.Han, S.X. Zhou, *J. Alloys Compd*. 477 (2009) 262–266.
7. J. Lang, J. Huot, *J. Alloys Compd*. 509 (2011) 18–22.

8. S. Kalinichenka, L. Rontzsch, T. Riedl, T. Gemming, T. Wei Bgarber, B. Kieback, *Int. J. Hydrogen Energy* 36 (2011) 1592–1600.
9. Huang Lin-jun, Wang Yan-xin, Tang Jian-guo, Liu Jing-quan, Wang Yao, Liu Ji-xian, Huang Zhen. *Int. J. Electrochem. Sci.* 6 (2011) 6200 - 6208.
10. Huang Lin-jun, Wang Yan-xin, Tang Jian-guo, Liu Jing-quan, Wang Yao, Liu Ji-xian. *Int. J. Electrochem. Sci.* 6 (2011) 5287 - 5297.
11. Lin-jun Huang, Jian-guo Tang, G.Y. Liang, Yao Wang, D.C. Wu. *J. Power Sources* 189 (2009) 1247-1250.
12. Lin-jun Huang, Jian-guo Tang, Yao Wang, Ji-xian Liu, D.C. Wu. *J. Alloys Compd*. 485 (2009) 186-191.
13. T.C. Hufnagel, *Nature Mater*. 3 (2004) 666-669.
14. T. Spassov, U. Koster, *J. Alloys Compd*. 287 (1999) 243-249.
15. Xuezhang xiao, Xinhua Wang, Linhui Gao, Li Wang, Changpin Chen, *J. Alloys Compd*. 413 (2006) 312-316.
16. B. Khorkounov, A. Gebert, Ch. Mickel, L. Schultz, *J. Alloys Compd*. 458 (2008) 479-485.
17. Z.M. Wang, H.Y. Zhou, Z.F. Gu, G. Cheng, A.B. Yu, *J. Alloys Compd*. 381 (2004) 234–239.
18. X. Xu, H.Y. Zhou, R.P. Zou, S.L. Zhang, Z.M. Wang, *J. Alloys Compd*. 396 (2005) 247–250.
19. M. Jurczyk, L. Smardz, I. Okonska, E. Jankowska, M. Nowak, K. Smardz, *Int. J.Hydrogen Energy* 33 (2008) 374–380.
20. M. Zhu, Y. Gao, Z.X. Che, Y.Q. Yang, C.Y. Chuang, *J. Alloys Compd*. 330–332 (2002)708-714.